Electronic Supplementary Material (ESI) for Physical Chemistry Chemical Physics.

Supplementary Information for:

Trimetallic Clusters in the Sumanene Bowl for Dinitrogen Activation

Ya-Ya Wang, Xun-Lei Ding*, Yan Chen, Meng-Meng Wang, Wei Li, and Xin Wang

*Author to whom correspondence should be addressed.
Email: dingxl@ncepu.edu.cn.

Table of Contents

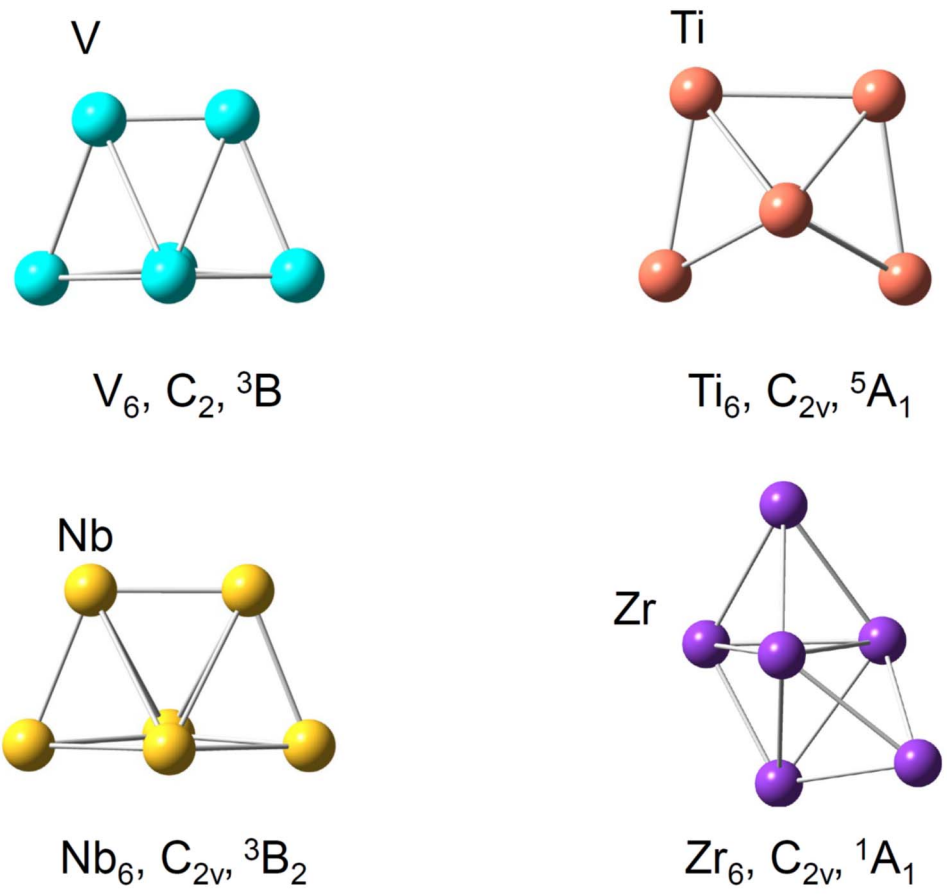

Figure S1. DFT calculated the lowest-lying isomers of M_6 (M = Ti, Zr, V, and Nb). The symmetry and electronic structure of each isomer are listed.

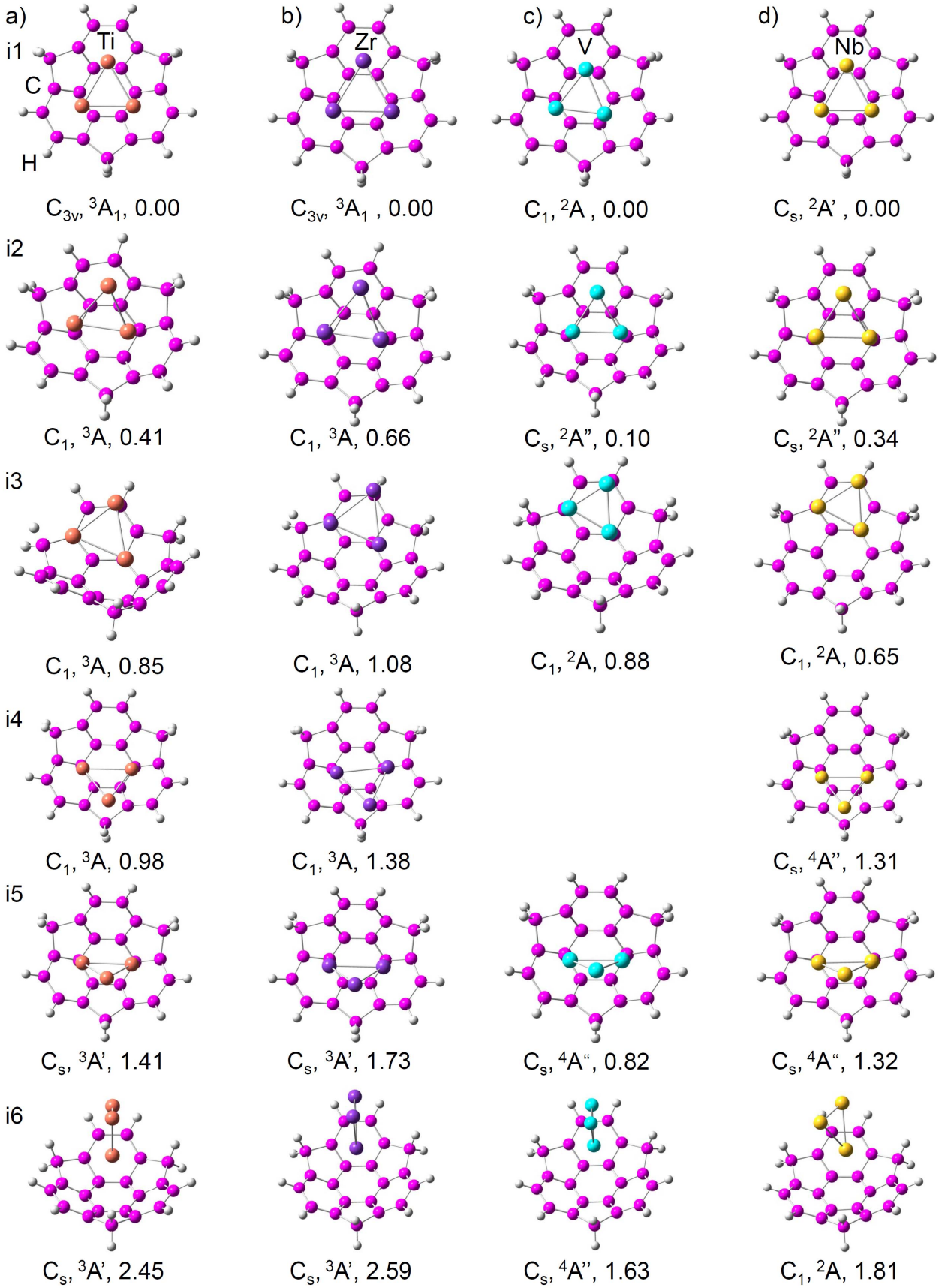

Figure S2. Low-lying stable structures of $C_{21}H_{12}$-M_3 with M_3 inside the bowl (denoted as i1-i6). Panels a), b), c), and d) are for M = Ti, Zr, V, and Nb, respectively. Relative energies with respect to the most stable structure are listed in eV.

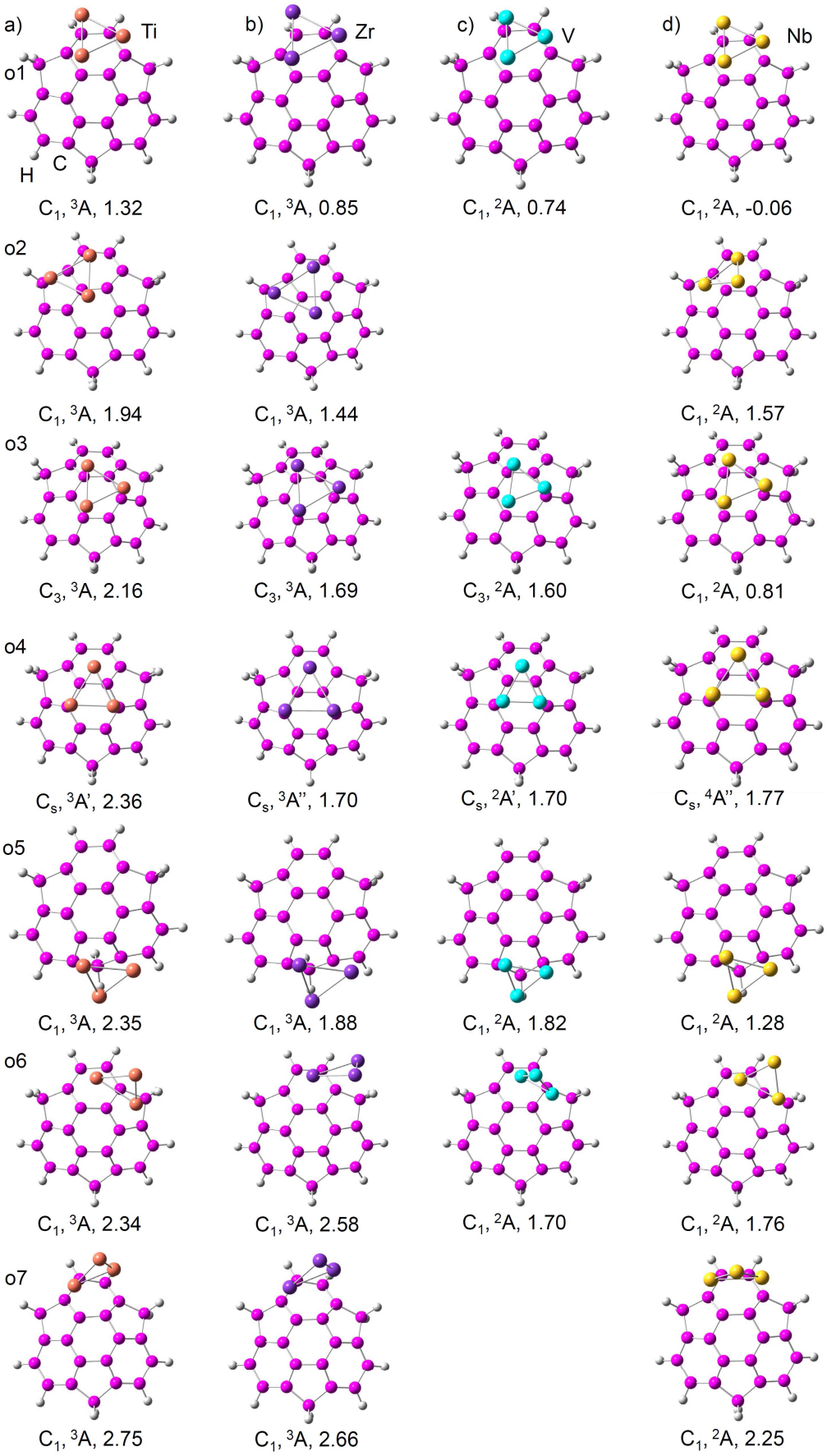

Figure S3. Low-lying stable structures of $C_{21}H_{12}$-M_3 with M_3 outside the bowl (denoted as o1-o7). Panels a), b), c), and d) are for M = Ti, Zr, V, and Nb, respectively. Relative energies with respect to the most stable structure are listed in eV.

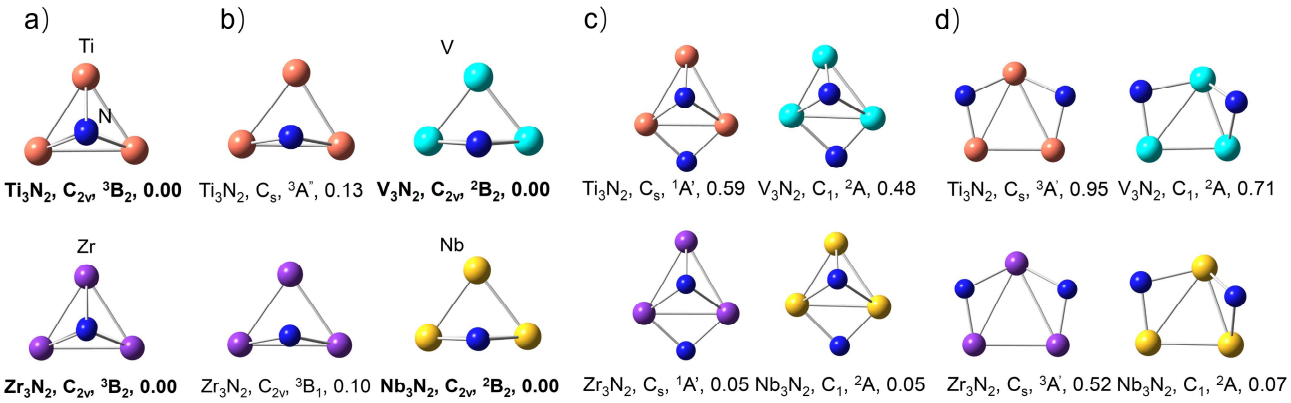

Figure S4. DFT calculated possible N–N dissociation products for reactions of M_3 (M = Ti, Zr, V, and Nb) and N_2. The symmetry and electronic structure of each isomer are listed, and the relative energies of each structure are in eV.

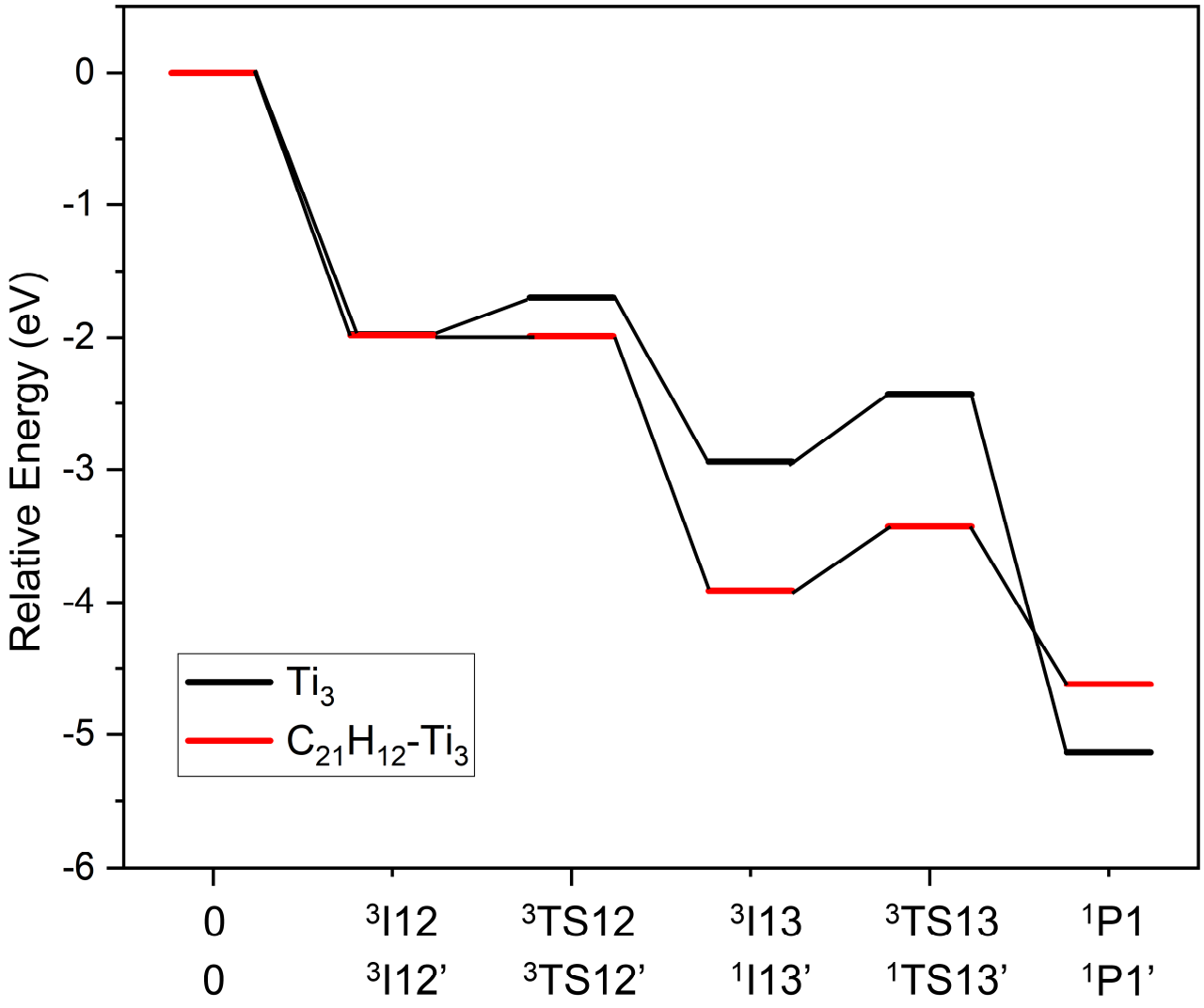

Figure S5. DFT calculated potential-energy profiles of the reaction pathways of N_2 dissociation on Ti_3 and $C_{21}H_{12}$-Ti_3. Relative energies with respect to the separated reactants are given in eV.

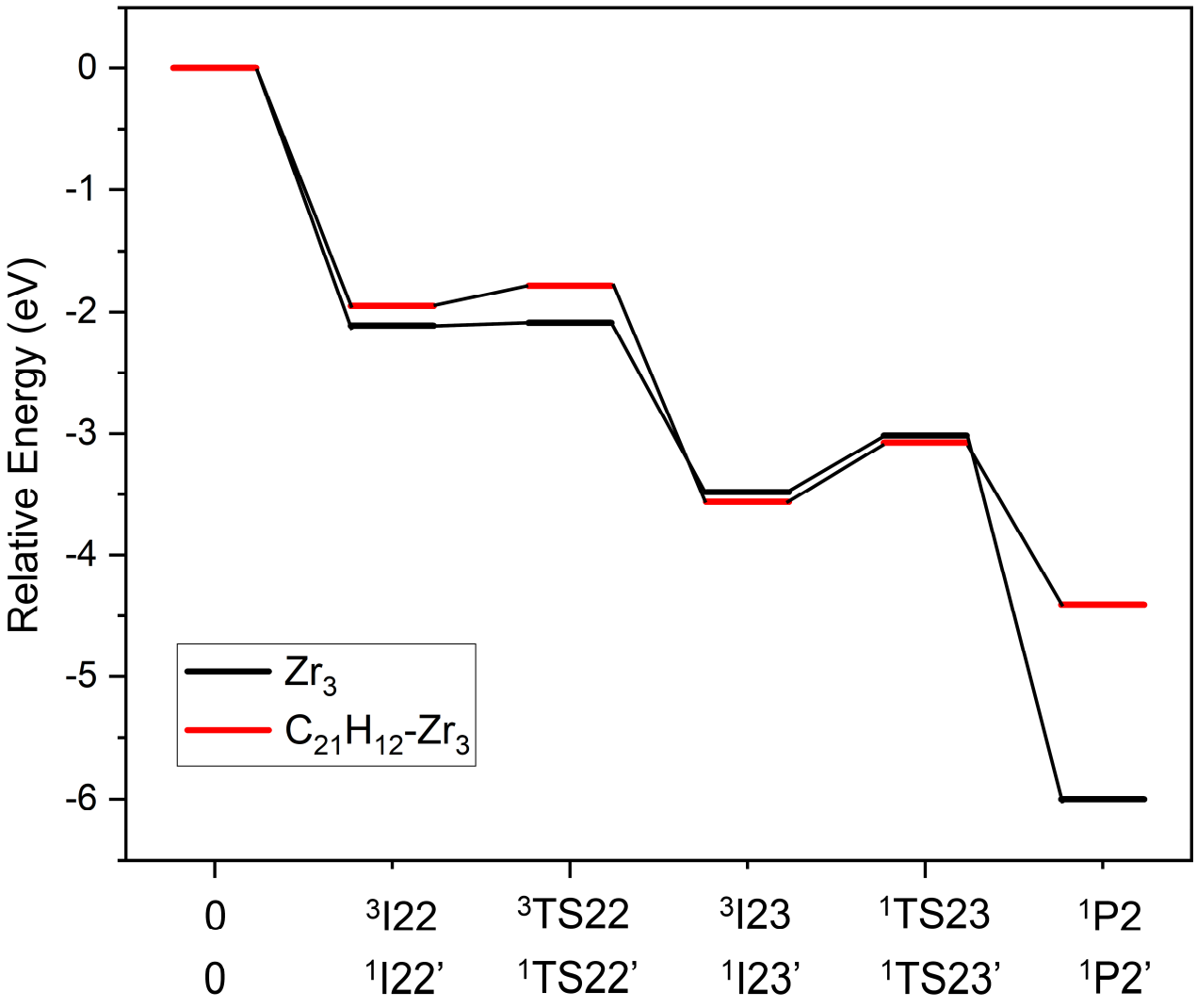

Figure S6. DFT calculated potential-energy profiles of the reaction pathways of N_2 dissociation on Zr_3 and $C_{21}H_{12}$-Zr_3. Relative energies with respect to the separated reactants are given in eV.

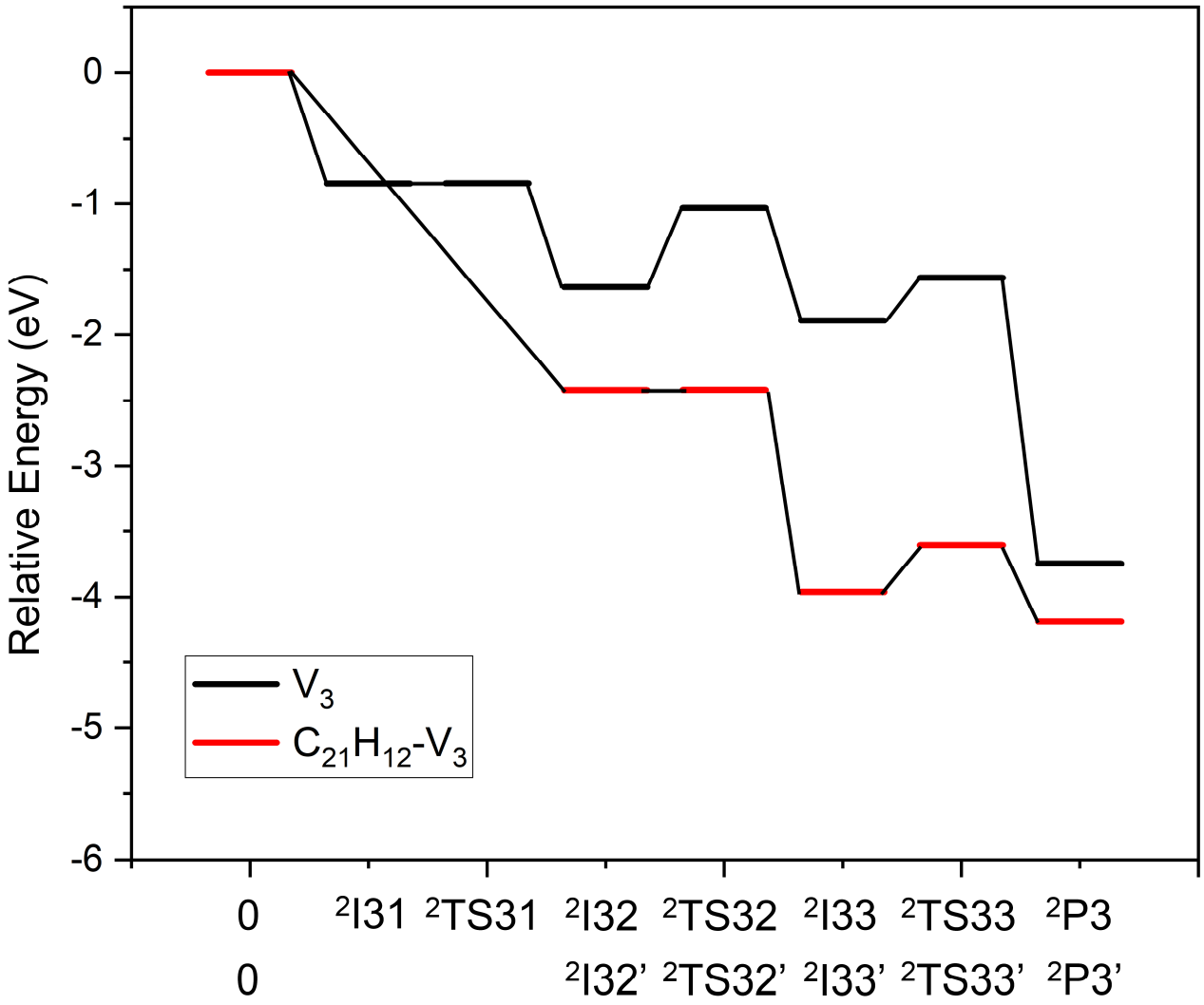

Figure S7. DFT calculated potential-energy profiles of the reaction pathways of N_2 dissociation on V_3 and $C_{21}H_{12}$-V_3. Relative energies with respect to the separated reactants are given in eV.

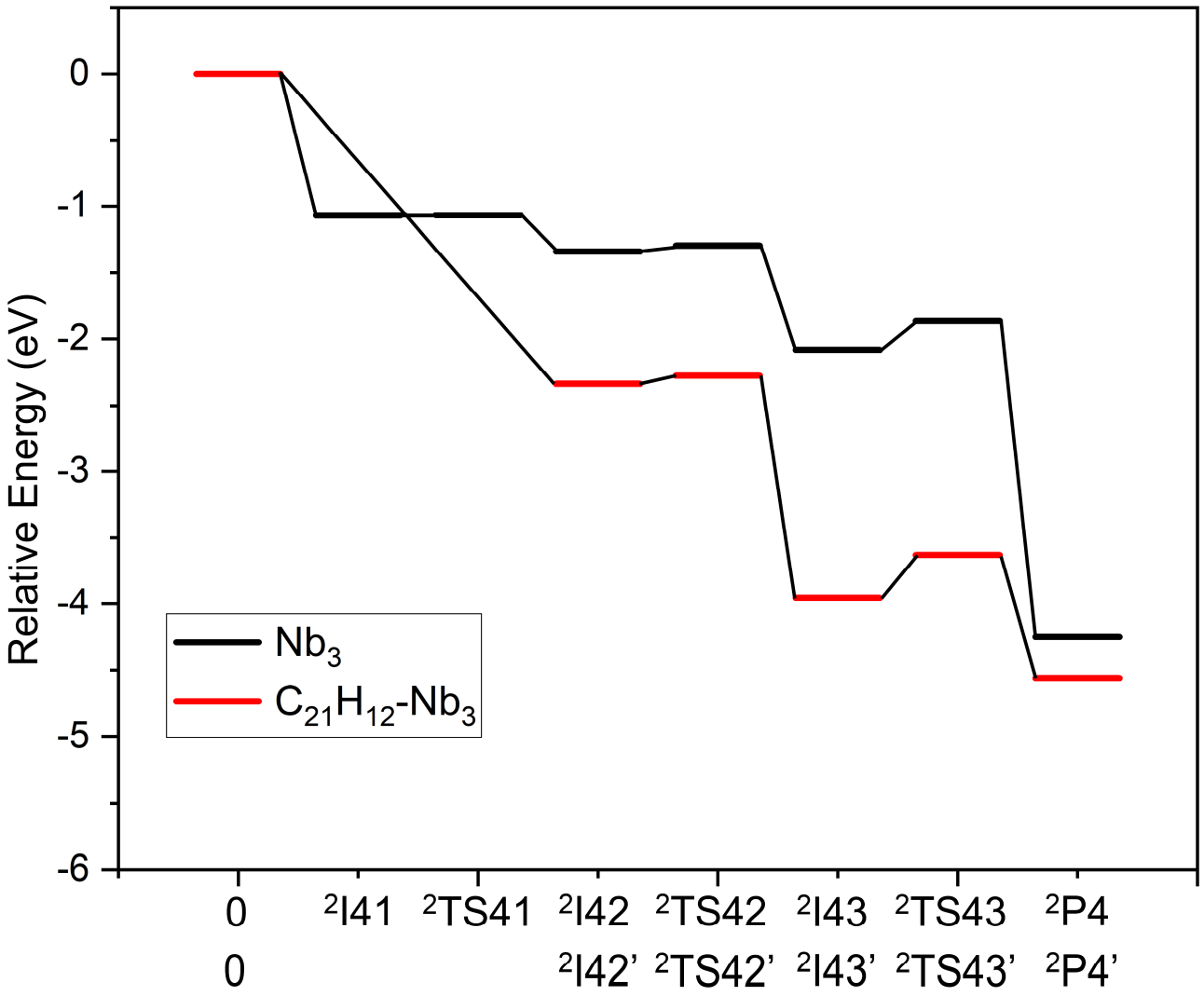

Figure S8. DFT calculated potential-energy profiles of the reaction pathways of N_2 dissociation on Nb_3 and $C_{21}H_{12}$-Nb_3. Relative energies with respect to the separated reactants are given in eV.

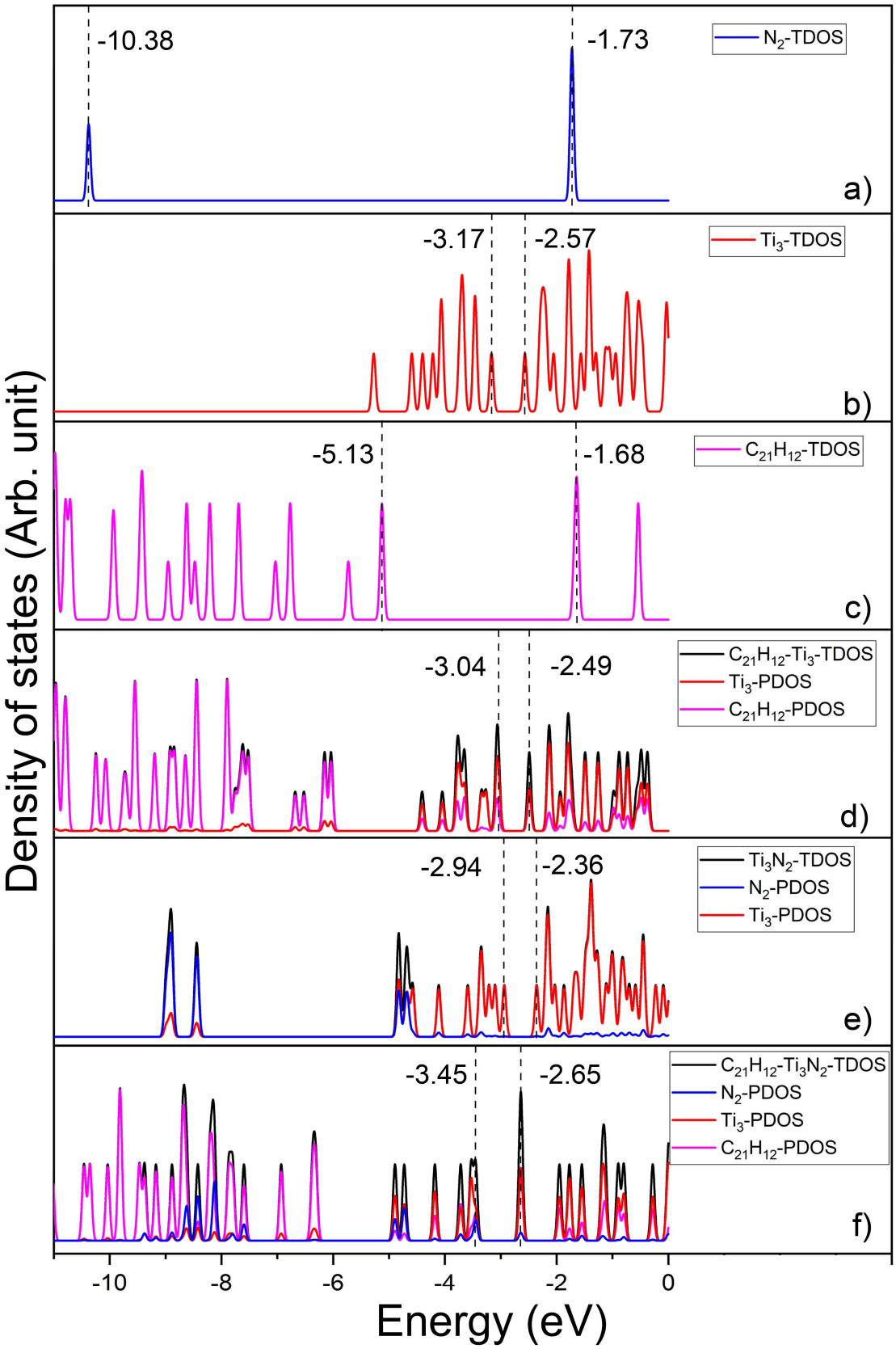

Figure S9. Density of state (DOS) of a) N_2, b) Ti_3, c) $C_{21}H_{12}$, d) $C_{21}H_{12}$-Ti_3, e) Ti_3N_2, and f) $C_{21}H_{12}$-Ti_3N_2, respectively. The total DOS (TDOS) and partial DOS are shown. The vertical dashed lines indicate the positions of the HOMO (left) or LUMO (right) in each panel, together with the values labelled in eV.

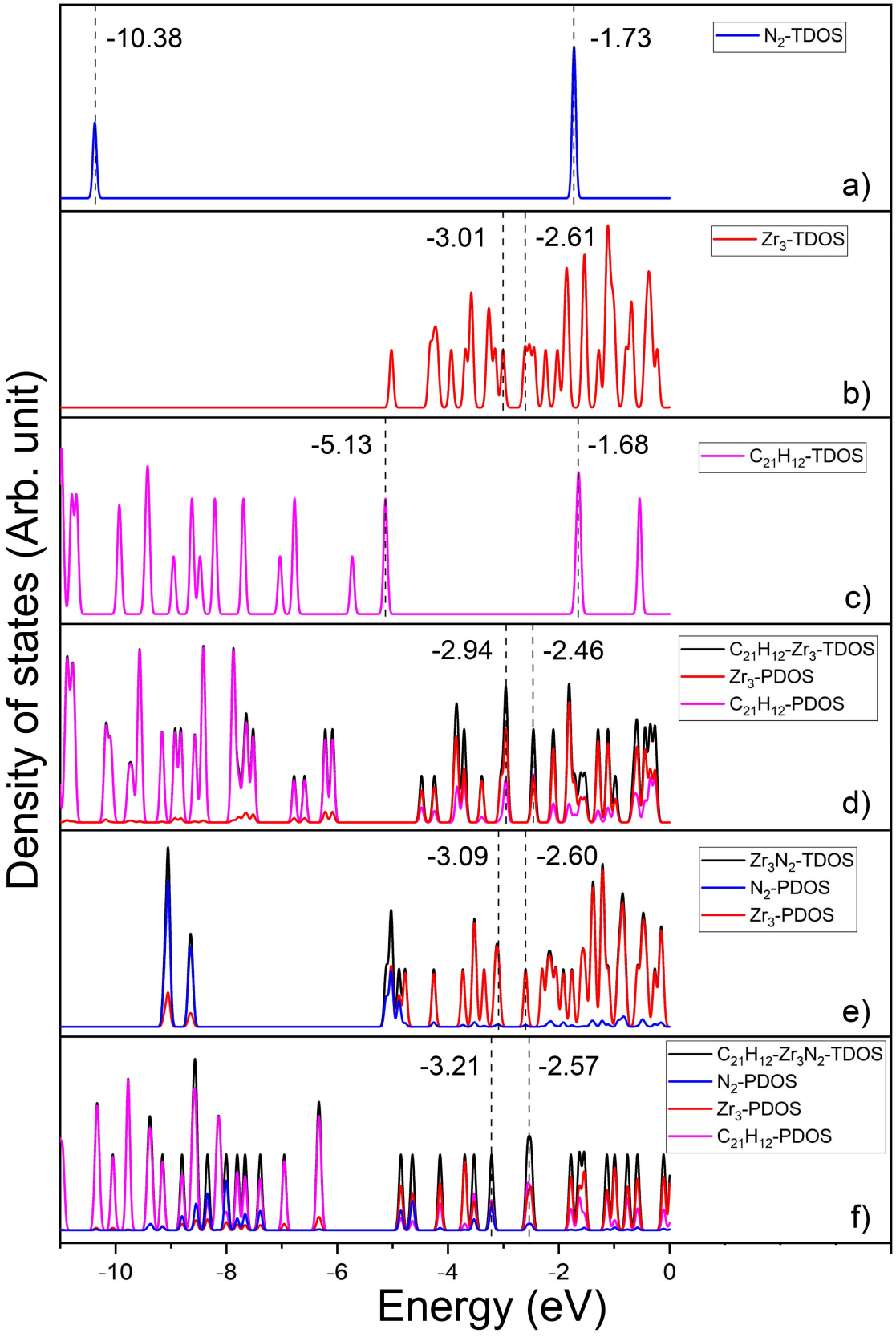

Figure S10. Density of state (DOS) of a) N_2, b) Zr_3, c) $C_{21}H_{12}$, d) $C_{21}H_{12}$-Zr_3, e) Zr_3N_2, and f) $C_{21}H_{12}$-Zr_3N_2, respectively. The total DOS and partial DOS are shown. The vertical dashed lines indicate the positions of the HOMO (left) or LUMO (right) in each panel, together with the values labelled in eV.

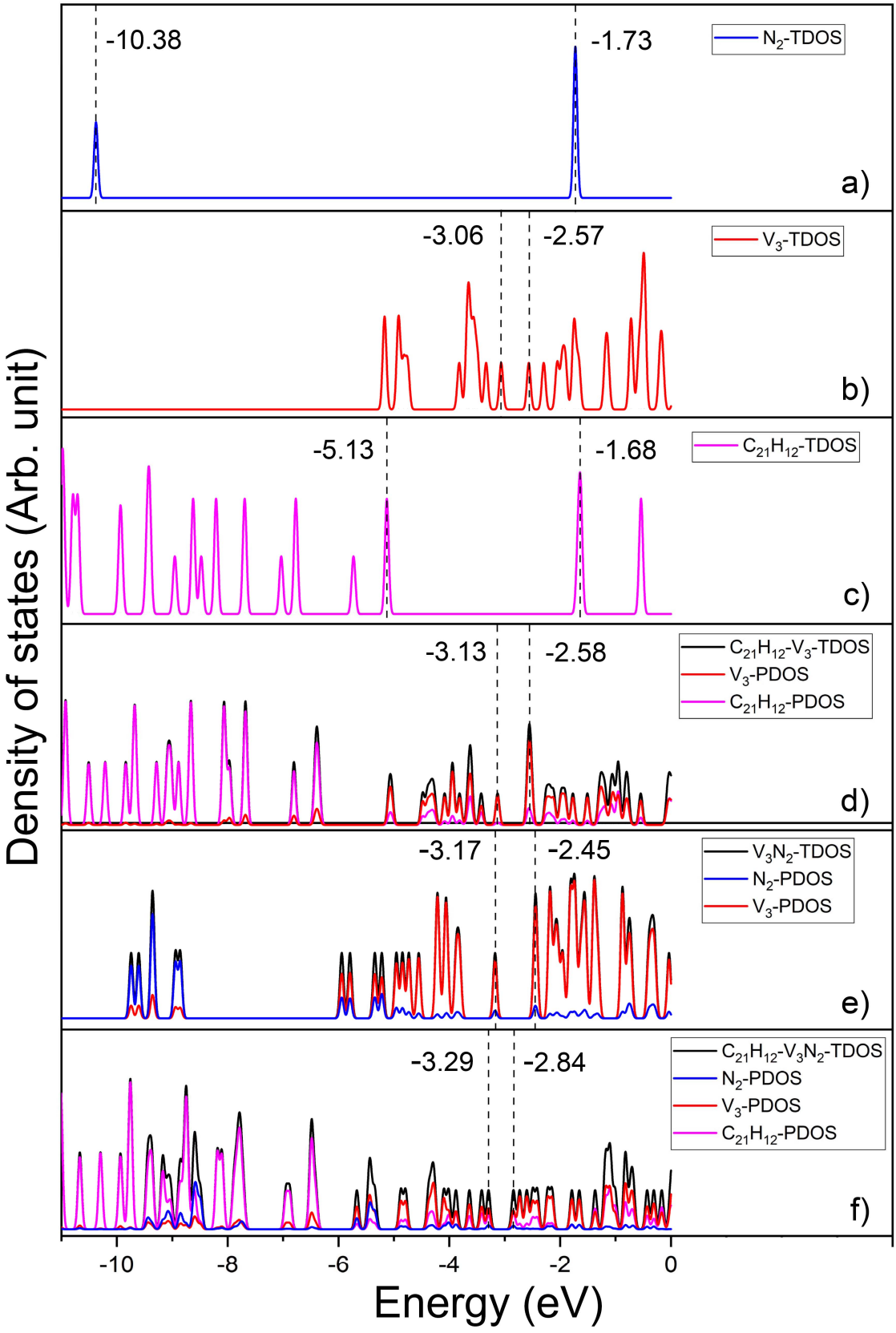

Figure S11. Density of state (DOS) of a) N_2, b) V_3, c) $C_{21}H_{12}$, d) $C_{21}H_{12}$-V_3, e) V_3N_2, and f) $C_{21}H_{12}$-V_3N_2, respectively. The total DOS and partial DOS are shown. The vertical dashed lines indicate the positions of the HOMO (left) or LUMO (right) in each panel, together with the values labelled in eV.

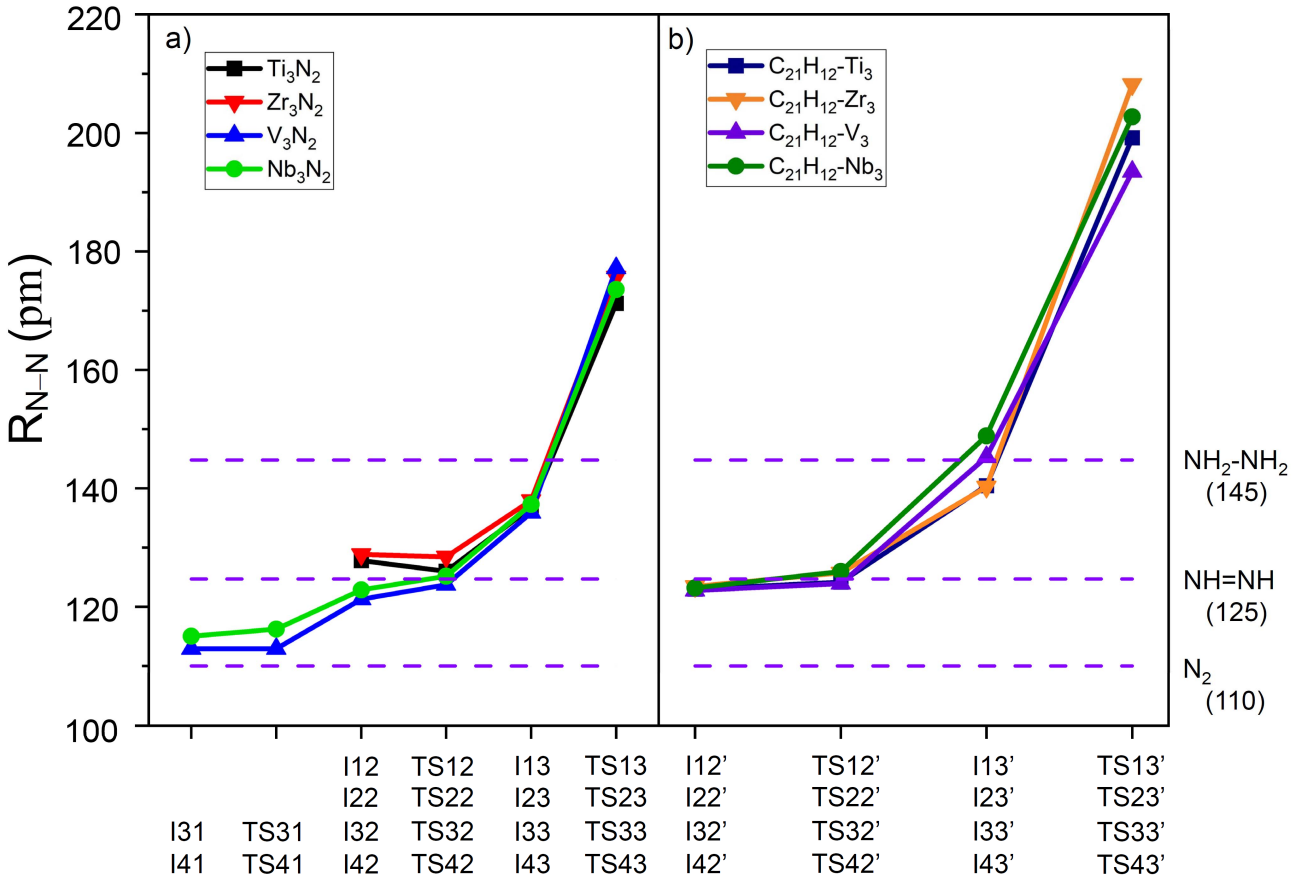

Figure S12. Calculated N−N bond lengths (R_{N-N}) of N_2 moiety in reaction intermediates and transition states for a) M_3 and b) $C_{21}H_{12}$-M_3 (M=Ti, Zr, V, and Nb). As references, three horizontal lines indicate the R_{N-N} of the triple, double, and single N–N bonds in free N_2, N_2H_2, and N_2H_4, respectively, with their calculated R_{N-N} values in brackets.

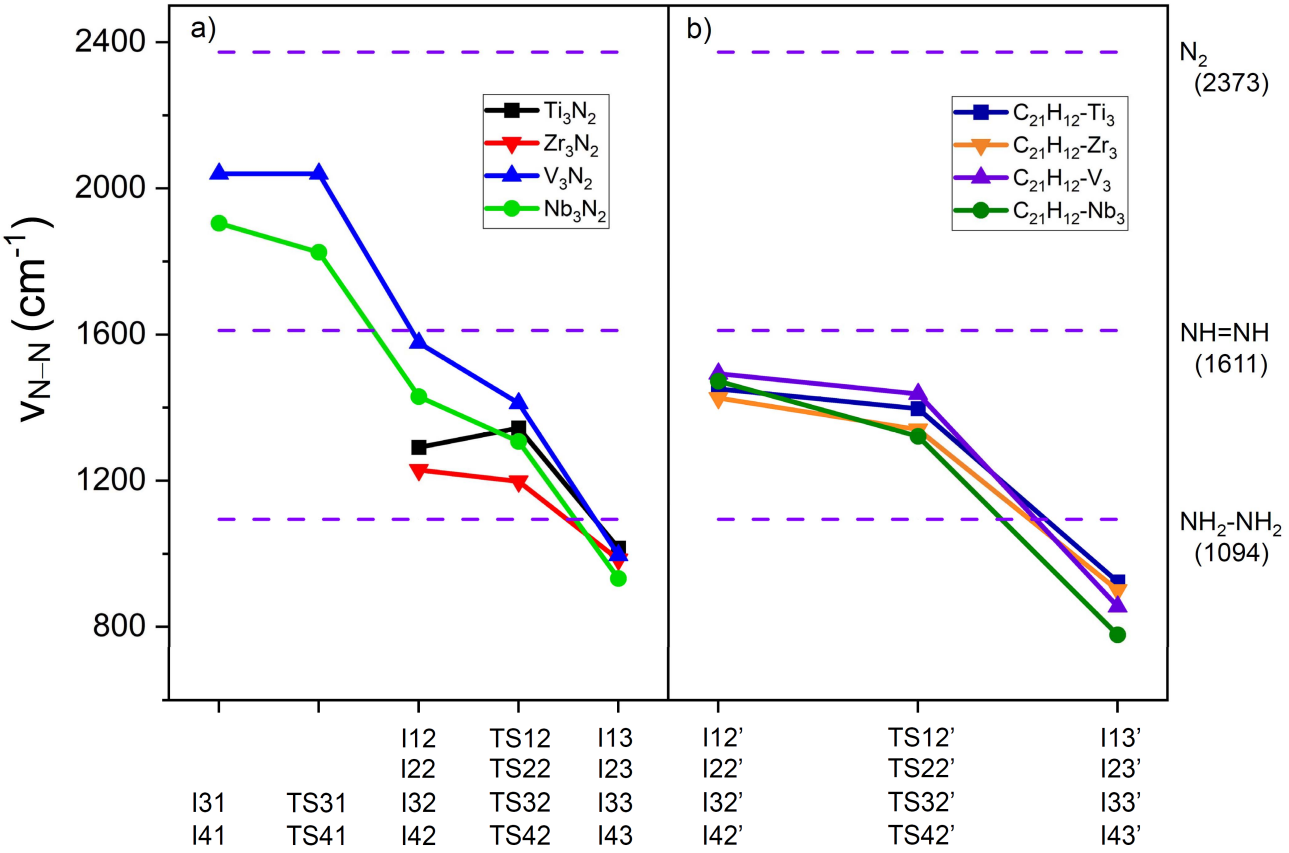

Figure S13. Calculated vibrational frequencies (ν_{N-N}) of N_2 moiety in reaction intermediates and transition states for a) M_3 and b) $C_{21}H_{12}$-M_3 (M = Ti, Zr, V, and Nb). As references, three horizontal lines indicate the ν_{N-N} of the triple, double, and single N–N bonds in free N_2, N_2H_2, and N_2H_4, respectively, with their calculated ν_{N-N} values in brackets.

Table S1. The metal bond lengths ($R_{M–M}$) of M_3, $C_{21}H_{12}$-M_3, and corresponding intermediates and transition states in the rate-determining step of N_2 transfer. $\Delta R_{M–M}$ is the difference of $R_{M–M}$ between the intermediate and the transition state. All bond lengths are in pm.

Clusters		$R_{M–M}$		Clusters		$R_{M–M}$	
Ti_3	245	207	245	$C_{21}H_{12}$-Ti_3	260	260	260
I12	252	206	260	I12’	268	267	270
TS12	254	231	259	TS12’	259	257	267
$\Delta R_{M–M}$	2	25	–1	$\Delta R_{M–M}$	–9	–10	–3
Zr_3	261	261	268	$C_{21}H_{12}$-Zr_3	287	287	287
I22	277	250	288	I22’	292	296	297
TS22	279	256	281	TS22’	279	293	301
$\Delta R_{M–M}$	2	6	–7	$\Delta R_{M–M}$	–13	–3	4
V_3	225	175	225	$C_{21}H_{12}$-V_3	237	240	241
I32	240	181	225	I32’	239	265	263
TS32	234	198	228	TS32’	238	264	257
$\Delta R_{M–M}$	–6	17	3	$\Delta R_{M–M}$	–1	–1	–6
Nb_3	241	226	241	$C_{21}H_{12}$-Nb_3	266	272	272
I42	246	240	245	I42’	264	278	292
TS42	246	239	243	TS42’	267	273	289
$\Delta R_{M–M}$	0	–1	–2	$\Delta R_{M–M}$	3	–5	–3

More detailed description of the reaction processes of N_2 on M_3 (M = Zr, V, and Nb)

The reaction process of Zr_3 and N_2 is similar to that of $Ti_3 + N_2$ (Figure 4b). Two spin flips (CP3 and CP4) are needed to reduce the spin multiplicity from $^5Zr_3$ to the first adsorption complex (^{3}I22), and then to the dissociation transition state ^{1}TS23. Compared with Ti_3, the transfer of N_2 on Zr_3 is even easier with an energy barrier of only 0.02 eV (^{3}I22→^{3}TS22), while the N–N dissociation step, the rate-determining step, still requires a high barrier of 0.46 eV (c.f. 0.51 eV of Ti_3). The reaction $Zr_3 + N_2$ (−6.00 eV) is also more exothermic than $Ti_3 + N_2$ (−5.13 eV). So Zr_3 may be a little more reactive than Ti_3 towards N_2.

The reaction processes of V_3/$Nb_3 + N_2$ are shown in Figures 4 c and d, respectively. Some different situations are found for these two systems compared with previous ones. Firstly, the whole reaction processes are always in a low spin state (doublet), so spin flips are no longer needed. Secondly, additional stable adsorption complexes with N_2 terminal end-on coordination on one metal atom can be obtained for V_3 (I31) and Nb_3 (I41). The N_2 molecule in this structure can transfer to the bridging ES on two metal atoms, as in Ti_3/$Zr_3 + N_2$, with negligible energy barriers (< 0.01 eV). Thirdly, for $V_3 + N_2$, the overall rate-determining step is the transfer of N_2 from I32 to TS32 (0.60 eV), which is higher than the N–N dissociation barrier of 0.33 eV (I33→TS33). Although the N–N dissociation on V_3 is more accessible than on Ti_3 and Zr_3, the transfer barrier on V_3 is 0.1 eV higher than the N–N dissociation barriers on Ti_3 and Zr_3. So V_3 is less reactive than Ti_3 and Zr_3. On the other hand, the N–N dissociation barrier on Nb_3 (I43→TS43, 0.21 eV) is even lower than that on V_3, and the energy barrier of N_2 transfer on Nb_3 (I42→TS42) is also small (0.04 eV). Therefore, Nb_3 is suggested to have the highest reactivity towards N_2, with low energy barriers for both N_2 transfer and N–N dissociation. The last different situation is for the reaction of $Nb_3 + N_2$, whose dissociation product has a different structure in which two N atoms occupy two bridge sites, respectively.